



HAL
open science

Fluorescent chitosan-based nanohydrogels and encapsulation of gadolinium MRI contrast agent for magneto-optical imaging

Juliette Moreau, Maité Callewaert, Volodymyr Malyskyi, Céline Henoumont, Sorina Voicu, Miruna Stan, Michael Molinari, Cyril Cadiou, Sophie Laurent, Françoise Chuburu

► To cite this version:

Juliette Moreau, Maité Callewaert, Volodymyr Malyskyi, Céline Henoumont, Sorina Voicu, et al.. Fluorescent chitosan-based nanohydrogels and encapsulation of gadolinium MRI contrast agent for magneto-optical imaging. *Carbohydrate Polymer Technologies and Applications*, 2021, 2, pp.100104. 10.1016/j.carpta.2021.100104 . hal-03523383

HAL Id: hal-03523383

<https://hal.univ-reims.fr/hal-03523383>

Submitted on 2 Aug 2023

HAL is a multi-disciplinary open access archive for the deposit and dissemination of scientific research documents, whether they are published or not. The documents may come from teaching and research institutions in France or abroad, or from public or private research centers.

L'archive ouverte pluridisciplinaire **HAL**, est destinée au dépôt et à la diffusion de documents scientifiques de niveau recherche, publiés ou non, émanant des établissements d'enseignement et de recherche français ou étrangers, des laboratoires publics ou privés.



Distributed under a Creative Commons Attribution - NonCommercial 4.0 International License

1 **Highlights:**

- 2 • Control of fluorophores (rhodamine and fluorescein) grafting onto chitosan backbone
3 by a combination of DOSY and fluorescence analyses.
- 4 • Fluorescent nanohydrogel syntheses by ionotropic gelation between grafted chitosans
5 and hyaluronic acid.
- 6 • The encapsulation of gadolinium chelate in these fluorescent nanohydrogels
7 considerably improves the detection sensitivity and thus the contrast in MRI imaging,
- 8 • These fully biocompatible magneto-optical nanohydrogels behave as hypersensitive
9 MRI probes in T_1 - and T_2 - modes while emitting a green or red light in optical
10 imaging.

11 **Abstract**

12 In the field of medical imaging, multimodal nanoparticles combining complementary imaging
13 modalities can give rise to new forms of imaging techniques that are able to make diagnosis
14 more precise and confident. In this context, resolution and sensitivity have often to be
15 gathered into a single imaging probe, by combination of MRI and optical imaging for
16 instance. Gadolinium chelate (Gd-CAs) loaded nanohydrogels, obtained from chitosan (CS)
17 and hyaluronic acid (HA) matrix, have shown their efficiency to greatly improve MRI
18 contrast ($r_1 \geq 80 \text{ mM}^{-1} \text{ s}^{-1}$). In this study, nanohydrogels were made intrinsically fluorescent
19 by chitosan pre-functionalization and a series of fluorescent chitosans were obtained by
20 covalent grafting of rhodamine (Rhod: $6.3\mu\text{M}$) or fluorescein (Fluo: $7.3\mu\text{M}$) tags. By
21 combining DOSY and fluorescence data, fluorescent chitosans (CS-Rhod and CS-Fluo) with a
22 low degree of substitution were then selected and used to encapsulate high gadolinium
23 loadings to obtain efficient magneto-optical nanohydrogels.

24

25 **Introduction**

26 Because of its excellent resolution and the absence of patient exposition to ionizing
27 radiations, MRI plays a central role in the arsenal of imaging techniques available to
28 radiologists. This technique is recognized for its excellent resolution but suffers from a lack of
29 sensitivity and information obtained from a simple unenhanced MR image is often not
30 sufficient to highlight the areas of interest in tissues. Usually, this drawback is compensated
31 by the injection of paramagnetic substances, in practice gadolinium chelates GdCAs (such as
32 gadoteric acid also known as DOTAREM®) at high concentration $> 0.1 \text{ mmol mL}^{-1}$, whose

1 role is to selectively highlight abnormal tissues by shortening the longitudinal relaxation times
2 of water protons in these tissues (Merbach, Helm & Toth, 2013). Until recently, GdCAs were
3 considered as safe but since the incidence of nephrogenic systemic fibrosis (NSF disease) in
4 patients with unpaired renal function (Rogosnitzky & Branch, 2016) and the observation of
5 MRI brain abnormalities, even with patients with normal renal function (Kanda et al., 2016),
6 the problem is now quite different. Elemental analyses of tissues collected after autopsy of
7 animal models have shown that these manifestations are correlated to *in vivo* Gd
8 demetallation, favored by the lack of chemical inertia of certain GdCAs (of linear structure,
9 that have been since withdrawn from the market) (Gianolio et al., 2017). However, there is
10 currently no clinically available alternative to injecting GdCA during MRI examinations,
11 when it is necessary (Gupta et al., 2020). The alternative is then needed to improve the
12 efficacy of low-risk GdCA to enhance the MRI signal. It is also important to keep in mind
13 that even if MRI provides images with an excellent resolution, it suffers from low sensitivity
14 detection.

15 A solution is to take advantage of nanoparticle strategy, not only to boost the intrinsic efficacy
16 of GdCAs (defined by their relaxivity r_1 in $\text{mM}^{-1} \text{s}^{-1}$) and to convert them into hypersensitive
17 MRI probes, but also to add an optical imaging modality by introduction of fluorophores in
18 the nanoassembly. We have demonstrated that the confinement of a low-risk GdCA such as
19 HGdDOTA (Gadolinium(III)-1.4.7.10-Tetraazacyclododecane-1.4.7.10-tetraacetate, which is
20 the active substance of DOTAREM®) into a nanogel (NG) matrix constituted with
21 polysaccharide biopolymers such as chitosan CS and hyaluronic acid HA (Courant et al.,
22 2012; Callewaert et al., 2014) can provide an interesting alternative to greatly increase the
23 MRI efficacy of GdCAs. Not only do they have the advantage over types of nanogels (Lux et
24 al., 2013; Soleimani et al., 2013) to overcome the sensitivity disadvantage of Gd contrast
25 agents (Washner et al., 2019) but they are also biocompatible with a low toxicity which is of
26 particular interest for biomedical applications.

27 Nanogels are water-rich nanoparticles, which is essential to exalt the MRI effect. The question
28 is therefore to know if it is possible to make them fluorescent, without the light emission
29 being reduced. Indeed, their emission may be quenched due to both the high concentration of
30 water OH vibrators (Mei et al., 2021) and metal ions in paramagnetic GdCAs (Asberg et al.,
31 2004) within the nanogels. These nanogels can be made fluorescent by polymer pre-
32 functionalization. In this work, we have chosen to make these nanogels fluorescent by CS
33 pre-functionalization. CS backbone was modified at the primary amino group of the
34 deacetylated CS units (at C-2, Scheme 1) with rhodamine (Rhod) or fluorescein (Fluo)

1 moieties. For that, we have taken advantage of the higher reactivity of the electronic lone pair
2 of CS primary amino group to graft rhodamine or fluorescein isothiocyanates (RBITC and
3 FITC respectively) *via* a thiourea linkage. Our objective being to involve those fluorescent CS
4 in ionic gelation, it is mandatory to control CS degree of substitution (DSCs) after
5 functionalization. Indeed, sufficient remaining positive charges are necessary on fluorescent
6 CS backbone to perform subsequent ionic gelation with HA in the presence of an ionogenic
7 cross linker (Gupta & Jabrail, 2006; Sang et al., 2020). Therefore, CS functionalization with
8 rhodamine and fluorescein has to be carefully characterized, especially in the absence of an
9 unambiguous marker of the thiourea bond (Ma et al., 2008). In this context, a series of CS-
10 fluorophore conjugates (CS-Rhod or CS-Fluo conjugates) were synthesized in which the level
11 of Rhod or Fluo substitution was systematically varied and quantified by a combination of
12 fluorescence and DOSY experiments. CS-fluorophores conjugates were then involved in
13 nanogel synthesis in the presence of GdCAs and after detailed morphological and
14 toxicological characterizations, the efficacy of the corresponding fluorescent Gd nanogels as
15 potential magneto-optical nanoprobe was explored.

16 1. Materials and Methods

17 1.1. Materials

18 Chitosan (CS, from shrimp shells, 51 kDa, viscosity = 33mPa.s in 1% acetic acid, 20°C) was
19 purchased from Sigma-Aldrich. A deacetylation degree (DD) of 86% was determined by ¹H
20 NMR spectroscopy according to published procedures. (Hirai et al., 1991; Vårum et al., 1991)
21 For calculations, CS repetitive unit (rep unit) molecular mass in which CS DD was taken into
22 account, was considered to be M_w in average ($CS_{rep\ unit} = 200\ g.mol^{-1}$) (Courant et al., 2012).
23 Hyaluronic acid sodium salt (HA 1000 kDa extracted from *Streptococcus equi sp*), Rhodamine
24 B isothiocyanate (RBITC, No. R1755), Fluorescein isothiocyanate (FITC), acetic acid and
25 sodium acetate were purchased from Sigma-Aldrich. Sodium tripolyphosphate (TPP) was
26 purchased from Acros Organics. DCl (35 wt % in D₂O) and D₂O were provided from Sigma-
27 Aldrich and Euriso-top, respectively. HGdDOTA (Gadolinium(III)-1.4.7.10-
28 Tetraazacyclododecane-1.4.7.10-tetraacetate) was synthesized according a published
29 procedure (Courant et al., 2012).

30 Fetal bovine serum (FBS), heat inactivated was purchased from Gibco by Life Technologies
31 (New Zealand), Roswell Park Memorial Institute (RPMI) 1640 medium and Dulbecco's
32 Modified Eagle's Medium (DMEM) from Gibco (Invitrogen, Grand Island, N.Y., USA), 3-
33 (4,5-dimethylthiazol-2-yl)-2,5-diphenyltetrazolium bromide (MTT), *In Vitro* Toxicology

1 Assay Kit Lactic Dehydrogenase based and antibiotics (penicillin, streptomycin and
2 amphotericin B) were provided by Sigma-Aldrich (St. Louis, MO, USA). Sterile water for
3 injections (Laboratoire Aguettant, Lyon, France) was systematically used for polymer,
4 nanoparticle preparations and analyses.

5 All products were used as received, without further purification.

6 Native and functionalized polymers (CS, CS-Rhodamine namely CS-Rhod and CS-
7 Fluorescein namely CS-Fluo, respectively) were characterized by FTIR (Nicolet IS 5
8 spectrometer equipped with an ATR ID5 module), ^1H NMR (Bruker Avance III 500 MHz
9 NMR spectrometer) at 318 K with $\text{D}_2\text{O}/\text{DCl}$ (700/1, v/v) as solvent, UV-visible and
10 fluorescence spectroscopies (Varian Cary 5000 Shimadzu UV-2401PC and Varian Cary
11 Eclipse, respectively). Centrifugation experiments were performed with an Alegra X-30
12 centrifuge (Beckman-Coulter).

13 The diffusion coefficients of different materials (CS, RBITC, FITC, CS-Rhod and CS-Fluo)
14 were determined by DOSY experiments (Diffusion Ordered Spectroscopy) on a Bruker
15 Avance II 500 MHz NMR spectrometer.

16 *2.2. Preparation, IR and ^1H NMR characterizations of CS-Rhodamine and CS-Fluorescein* 17 *polymers*

18 *2.2.1. CS-Rhodamine (CS-Rhod) synthesis*

19 CS (200 mg, 1.0 mmol of NH_2 function) was dissolved under N_2 atmosphere in 10 mL of an
20 aqueous solution of acetic acid 1% (v/v). After complete CS dissolution, the pH was adjusted
21 to 5 by addition of 1M NaOH and 5 mL of MeOH was added and the resulting solution
22 allowed to stir for 3h (Ma et al., 2008). Then, different stoichiometric ratios of RBITC were
23 added in anhydrous MeOH to the CS solution (RBITC/ NH_2 CS molar ratio expressed as %
24 mol $(\text{NCS}/\text{NH}_2)_{\text{initial}}$ of 2, 5 and 10%, corresponding to 11, 27 and 53 mg of RBITC in 3.5, 8
25 and 16 mL of anhydrous MeOH respectively). The RBITC solution was added dropwise to
26 the CS solution and the mixture was stirred under N_2 atmosphere, in the dark at room
27 temperature for 36h. At the end of the reaction, CS-Rhod was precipitated by using a NaOH
28 solution (1M), and the resulting precipitate washed with water for injection. The polymer was
29 recovered by centrifugation (6500 rpm, 12 min, at room temperature) and the overall
30 procedure repeated until waste water reached pH 7 and no fluorescence being detected in the
31 corresponding solution. CS-Rhod was finally obtained after freeze-drying as a pink-mauve
32 foam (between 120 and
33 180 mg according to the sample).

1 FT-IR (ATR, cm^{-1}): 3362 (ν_{OH} and ν_{NH}), 2871 (ν_{CH}), 1650 (amide I), 1559 (amide II), 1053,
2 1027 (pyranose ring).

3 ^1H NMR (500 MHz, 318K, $\text{D}_2\text{O}/\text{DCI}$: 700 $\mu\text{L}/1\mu\text{L}$), δ (ppm): 1.30 (t, CH_3 - Rhod), 2.07 (s,
4 CH_3 - CS acetyl units), 2.99 (s, 1H, CS), 3.37 (s, CH_2 - Rhod), 3.5-4.2 (m, 5H, CS), 4.71 (s,
5 1H, CS), 6.9-7.9 (aromatic H - Rhod).

6 2.2.2. CS-Fluorescein (*CS-Fluo*) synthesis

7 CS-Fluorescein (CS-Fluo) was synthesized according to the same procedure, *i.e.* from a CS
8 solution (mixture of acetic acid and anhydrous MeOH) and FITC solution (in anhydrous
9 MeOH). The same FITC/ NH_2 CS molar ratios were prepared namely 2, 5 and 10% (expressed
10 as % mol (NCS/NH_2)_{initial}) corresponding to 8, 20 and 40 mg of FITC in 3, 7.5 and 15 mL of
11 anhydrous MeOH respectively.

12 After precipitation (with 1 M NaOH) and washing with water for injection until pH 7, CS-
13 Fluo was finally obtained after freeze-drying as an orange foam (between 130 and 180 mg
14 according to the sample).

15 FT-IR (ATR, cm^{-1}): 3288 (ν_{OH} and ν_{NH}), 2874 (ν_{CH}), 1634 (amide I), 1573 (amide II), 1063,
16 1028 (pyranose ring).

17 ^1H NMR (500 MHz, 318K, $\text{D}_2\text{O}/\text{DCI}$: 700 $\mu\text{L}/1\mu\text{L}$), δ (ppm): 2.07 (s, CH_3 - CS acetyl units),
18 3.02 (s, 1H, CS), 3.5-4.2 (m, 5H, CS), 4.73 (s, 1H, CS), 6.5-8.0 (aromatic H - Fluo).

19 2.3. Determination of CS degree of substitution (DS_{CS}) by a combination of fluorescence 20 and DOSY experiments

21 In order to determine the degree of substitution of chitosan in CS-Rhod ($DS_{\text{CS}}^{\text{Rhod}}$) or CS-Fluo
22 ($DS_{\text{CS}}^{\text{Fluo}}$) samples, it was mandatory to distinguish between the grafted amount of fluorophore
23 (RBITC_G namely Rhod_G or FITC_G namely Fluo_G) and the ungrafted one (Rhod_{UG} or Fluo_{UG}).
24 For that, a combination of fluorescence spectroscopy and DOSY experiments was applied.

25 *Fluorescence spectroscopy*: The total amount of fluorophore (Rhod_T or Fluo_T) which
26 corresponded to the sum of the grafted fluorophore amount (Rhod_G or Fluo_G) and the
27 ungrafted one (Rhod_{UG} or Fluo_{UG}), was determined by fluorescence spectroscopy after sample
28 purification. For this purpose, we measured the emission intensities at 576 nm (rhodamine) or
29 511 nm (fluorescein) of 0.25-0.45 mg mL^{-1} solutions of CS-Rhod (or CS-Fluo), dissolved in
30 an aqueous solution of acetic acid 1% (v/v) and diluted 100 times with acetate buffer (pH 4.7)
31 (Varian Cary Eclipse spectrometer, with λ_{exc} = 550 and 450 nm for rhodamine and fluorescein

1 emission measurements respectively, and $\Delta\lambda_{exc} = \Delta\lambda_{em} = 5$ nm). The ratio of the total amount
 2 of fluorophore to chitosan (fluorophore_T/ CS) was calculated as the percent molar
 3 concentration of fluorophore to CS molar concentration according to Eq. 1.

$$4 \quad \% \left(\frac{\text{fluorophore}_T}{CS} \right)_{mol} = \frac{I_{\text{fluorophore}}/k_{\text{fluorophore}}}{m_{CS\text{-fluorophore}}/(M_{CS_{rep\ unit}} \times V)} \times 100 \quad \text{Eq. 1}$$

5 with $I_{\text{fluorophore}}$ being the emission intensity measured at 576 and 511 nm for CS-Rhod and CS-
 6 Fluo respectively, $k_{\text{fluorophore}}$ being equal to the ratio between the emission intensity (at 576 or
 7 511 nm) and the fluorophore concentration. $k_{\text{fluorophore}}$ was determined for rhodamine and
 8 fluoresceine by calibration with standard solutions of each fluorophore. Serial dilutions in
 9 acetate buffer (pH 4.7) of a stock methanolic solution of each fluorophore (150 mg mL⁻¹)
 10 were prepared to reach fluorophore concentrations ranging from 0.003 to 0.1 mg mL⁻¹. The
 11 corresponding proportionality coefficient determined were $k_{\text{Rhod}, 576 \text{ nm}} = 1.75 \times 10^9$ mol⁻¹L
 12 and $k_{\text{Fluo}, 511 \text{ nm}} = 4.58 \times 10^8$ mol⁻¹L.

13 *DOSY Experiments:* Due to the large difference between rhodamine (or fluorescein) and CS-
 14 Rhod (or CS-Fluo) molecular weights, it was expected to discriminate between ungrafted and
 15 grafted fluorophore, using their respective diffusion coefficients. For that, preliminary DOSY
 16 experiments were performed to determine CS, rhodamine (Rhod) and fluorescein (Fluo)
 17 diffusion coefficients (D_{CS} , D_{Rhod} and D_{Fluo} respectively). Bipolar gradient pulses with two
 18 spoil gradients were used to measure these coefficients (BPP-LED pulse sequence). The value
 19 of the gradient pulse length τ was 4 ms for CS and 2ms for Rhod and Fluo, while the value of
 20 the diffusion time Δ was set to 500 ms for CS and 250 ms for Rhod and Fluo. The pulse
 21 gradients were incremented in 16 steps from 2% to 95% of the maximum gradient strength
 22 (53.5 G/cm) in a linear ramp and the temperature was set at 30°C. CS, Rhod and Fluo
 23 diffusion curves were then extracted from DOSY spectra of CS (for the peak at
 24 $\delta = 2.1$ ppm), Rhod (for the peak at $\delta = 1.2$ ppm) and Fluo (for the peak at $\delta = 6.8$ ppm). In
 25 each case, the mono-exponential diffusion curves were fitted with Eq. 2 (Johnson, 1999;
 26 Augé, Amblard-Blondel & Delsuc, 1999) to obtain D_{CS} value of 5×10^{-12} m²s⁻¹, and D_{Rhod} and
 27 D_{Fluo} values of 2×10^{-10} m²s⁻¹ and 4×10^{-10} m²s⁻¹ respectively (Figure S4).

$$28 \quad I = I_0 \exp[-\gamma^2 g^2 D \delta^2 (\Delta - (\delta/3) - (\tau/2))] \quad \text{Eq. 2}$$

29 Then, similar DOSY experiments were performed with CS-Rhod and CS-Fluo. The diffusion
 30 curves were extracted from CS-Rhod and CS-Fluo DOSY spectra, for the more intense peak
 31 of Rhod and Fluo, at 1.3 and 6.8 ppm respectively. The diffusion curves that showed a

1 monoexponential evolution were fitted according to Eq. 2. The diffusion curves that exhibited
 2 a biexponential evolution were fitted according to Eq. 3, (Johnson, 1999; Augé, Amblard-
 3 Blondel & Delsuc, 1999)

$$4 \quad I = I_G \exp[-\gamma^2 g^2 D_G \mathcal{F}(\Delta - (\delta/3) - (\tau/2))] + I_{UG} \exp[-\gamma^2 g^2 D_{UG} \mathcal{F}(\Delta - (\delta/3) - (\tau/2))] \quad \text{Eq. 3}$$

5 where I_G and I_{UG} were the intensities at 0% gradient, for grafted and ungrafted fluorophore
 6 (Rhod or Fluo) respectively, γ the gyromagnetic ratio, g the gradient strength, D_G and D_{UG} the
 7 diffusion coefficients of grafted and ungrafted fluorophores respectively, δ the gradient pulse
 8 length, Δ the diffusion time and τ the interpulse spacing in the BPP-LED pulse sequence.

9 During the fitting, D_G and D_{UG} were then fixed to values measured independently on chitosan
 10 and rhodamine or fluorescein, respectively: $D_{CS} = 5 \times 10^{-12} \text{ m}^2\text{s}^{-1}$, $D_{Rhod} = 2 \times 10^{-10} \text{ m}^2\text{s}^{-1}$ and
 11 $D_{Fluo} = 4 \times 10^{-10} \text{ m}^2\text{s}^{-1}$.

12 I_G and I_{UG} values extracted from the fitting, allowed to calculate the percentage of grafted
 13 fluorophore over the total amount of fluorophore (fluorophore_G/fluorophore_T) (Eq. 4):

$$14 \quad \% \frac{\text{Fluorophore}_G}{\text{Fluorophore}_T} = \frac{I_G}{I_G + I_{UG}} \times 100 \quad \text{Eq. 4}$$

15 The percentage of fluorophore grafted to CS chains (DS_{CS}) was then calculated (Eq. 5) from
 16 emission measurements and DOSY experiments (from Eqs. 1 and 4):

$$17 \quad DS_{CS} = \% \left(\frac{\text{fluorophore}_G}{CS} \right) = \frac{I_{\text{fluorophore}}/k_{\text{fluorophore}}}{m_{CS\text{-fluorophore}}/(M_{CS_{rep\ unit}} \times V)} \times \frac{I_G}{I_G + I_{UG}} \times 100 \quad \text{Eq. 5}$$

18 where I_G and I_{UG} stand for the intensities extracted from the DOSY experiments, for grafted
 19 and ungrafted fluorophores (rhodamine or fluorescein) respectively.

20 *2.4. Preparation and characterization of CS–Rhod and CS–Fluo nanoparticles by ionic* 21 *gelation (CS–Rhod-TPP/HA and CS–Fluo-TPP/HA nanogels)*

22 *2.4.1. CS–Rhod-TPP/HA and CS–Fluo-TPP/HA nanogel syntheses*

23 Solutions of fluorescent CS were prepared by dissolution of CS-Rhod ($DS_{CS}^{Rhod} = 0.85\%$) or
 24 CS-Fluo ($DS_{CS}^{Fluo} = 0.86\%$) powders in citric acid (10% wt/v) solutions (2.5 mg mL⁻¹).

25 CS-fluorophore-TPP/HA nanogels (CS–Rhod-TPP/HA and CS–Fluo-TPP/HA NGs) were
 26 obtained by an ionotropic gelation process. For this purpose, the polyanionic aqueous phase
 27 (4.5 mL) containing both HA (0.8 mg mL⁻¹) and TPP (1.2 mg mL⁻¹) was added dropwise to
 28 the CS-fluorophore solution (9 mL) under sonication (750W, amplitude 32%). At the end of
 29 the addition, magnetic stirring was maintained for 10 min. Purification and pH correction of
 30 the nanosuspensions was then carried out by dialysis against water for injection (3 × 12h)

1 using a membrane of 25 kDa cut-off (Spectrum Lab) to reach physiological pH. Gadolinium-
2 loaded nanogels (GdDOTA \subset CS-Rhod-TPP/HA and GdDOTA \subset CS-Fluo-TPP/HA NGs) were
3 prepared in the same way, by incorporating HGdDOTA (17 mg) as the MRI contrast agent in
4 the anionic phase.

5 2.4.2. CS–Rhod and CS–Fluo nanogels characterization by Dynamic Light Scattering

6 The nanogels averaged hydrodynamic diameters (Z-ave) were determined by Dynamic Light
7 Scattering (DLS) with a Zetasizer Nano ZS (Malvern Zetasizer Nano-ZS, Malvern
8 Instruments, Worcestershire, UK). Each sample was analyzed in triplicate at 20 °C at a
9 scattering angle of 173°, after a 1/20 dilution in water. Water was used as a reference
10 dispersing medium.

11 ζ -(zeta) potential data were collected through Electrophoretic Light Scattering (ELS) at 20°C,
12 150 V, in triplicate for each sample, after a 1/20 dilution in water. The instrument was
13 calibrated with a Malvern – 68 mV standard before each analysis cycle.

14 2.4.3. In vitro cytotoxicity of CS-Rhod and CS-Fluo nanogels

15 RAW 267.4 and A20 cell lines were purchased from American Type Culture Collection
16 (ATCC catalog no., TIB-7 and TIB-208, respectively). RAW 267.4 cells (adherent cells) were
17 cultured in Dulbecco Modified Eagle Medium (DMEM) pH 7.4 with 4 mM L-glutamine
18 adjusted to contain 4.5 g L⁻¹ glucose and, 1.5 g L⁻¹ sodium bicarbonate. The growth medium
19 was supplemented with 10% fetal bovine serum, 1% antibiotics (penicillin, streptomycin,
20 amphotericin). The A20 cell line (murine B lymphocytes, from reticulum cell sarcoma in
21 suspension) were cultured in RPMI 1640 medium pH 7.4 with 2 mM L-glutamine, 1.5 g L⁻¹
22 Na₂CO₃, 4.5 g L⁻¹ glucose, 1 mM sodium pyruvate, 10 mM HEPES and supplemented with
23 10% fetal bovine serum and 1% antibiotics (penicillin, streptomycin, and amphotericin). All
24 cell types were maintained at 37°C in a humidified atmosphere (95%) with 5% CO₂.
25 The concentration of CS-Rhod-TPP/HA and CS-Fluo-TPP/HA stock nanosuspensions was
26 1.17 mg mL⁻¹ and the Gd concentration of GdDOTA \subset CS-Rhod-TPP/HA and GdDOTA \subset CS-
27 Fluo-TPP/HA stock nanosuspensions was 0.144 mM and 0.144 mM respectively. Dilutions
28 were then made in the culture medium for each cell line tested. In parallel, the cells seeded in
29 24-well plates at a density of 10⁵ cells mL⁻¹ for RAW 264.7 and 2×10⁵ cells mL⁻¹ for A20 cell
30 lines, were incubated for 6 and 24 hours at different concentrations of CS-Rhod-TPP/HA, CS-
31 Fluo-TPP/HA nanogels (*i.e.* 5, 15, 30, 60 and 120 μ g mL⁻¹) or GdDOTA \subset CS-Rhod-TPP/HA
32 and GdDOTA \subset CS-Fluo-TPP/HA nanogels (*i.e.* 0.5, 1, 2.5, 5 and 10 μ M of Gd).

1 Cell viability was measured by the MTT, 3-(4,5-dimethylthazol-2-yl)-2,5-diphenyl
2 tetrazolium bromide), assay. After the exposure time, the culture medium was removed and in
3 each well were added 500 μL MTT (1 mg mL^{-1}) for 2 hours. After that, the MTT solution was
4 removed and the formazan crystals were solubilized in 100% isopropanol. The optical density
5 was measured at 595 nm using Flex Station 3 Multi-Mode Microplate Reader. The cell
6 viability was expressed in percentage considering 100% viability for control cells.

7 The LDH release was measured in the culture media of treated cells using the *In Vitro*
8 Toxicology Assay Kit (Sigma-Aldrich, USA) and compared to the LDH release level of
9 control (untreated cells). After each exposure interval, a volume of 50 μL medium was taken
10 from each sample and placed on a 96-well microtiter plate and then 100 μL of assay mixture
11 were added. After 20-30 min at room temperature, the reaction was stopped by adding 1/10
12 volume of HCl 1 M and the enzymatic activity was determined spectrophotometrically using
13 the Flex Station 3 Multi-Mode Microplate Reader. The absorbance was read at 450 nm and
14 the results were expressed relative to control.

15 2.4.4. Fluorescent nanogels characterization by Atomic Force Microscopy (AFM) and 16 confocal microscopy

17 To obtain information about the different NP sizes and their fluorescent properties, correlative
18 experiments were performed using an Atomic Force Microscope (AFM) coupled to a confocal
19 microscope. Each sample was analyzed in triplicate at 20 °C after a 1/20 dilution in water. To
20 be observed, the NPs were deposited on a glass slide and after one hour, the samples were
21 rinsed with deionized water. All the experiments were performed in water to avoid nanogel
22 drying (and thus possible changes in their structures / morphologies).

23 First a confocal image was acquired using a Axio Observer 7 LSM 800 Airyscan microscope
24 (ZEISS, Germany). For the excitation wavelength, lasers at 561 and 488 nm were used for the
25 CS-Rhod-TPP/HA and CS-Fluo-TPP/HA nanogels, respectively. A 100 \times objective was used
26 and 512 pixels \times 512 pixels image were acquired. Then in a second time, areas with
27 fluorescent NPs were chosen and scanned with a Resolve AFM (BrukerNano, USA). Peak
28 Force Tapping Quantitative Nano-Mechanicals (PFT-QNM) mode was used to perform AFM
29 imaging of the different samples in liquid conditions. Nitride coated silicon cantilevers (SNL,
30 Bruker probes, USA) with a resonance frequency of 65 kHz, a nominal spring constant of
31 0.35 N/m and a tip radius of 6 nm were used for this work and were calibrated for each
32 experiment. Images were acquired with a scan rate of $\sim 1.0 - 1.5$ Hz, with a force kept as low
33 as possible (typically 0.5 nN or lower). Imaging gains were automatically optimized by the

1 software. The different AFM images were analyzed and processed with the Nanoscope
2 Analysis 2.0 software (BrukerNano, USA). At least, 5 different areas for each sample were
3 analyzed by AFM to determine averaged NP diameters.

4 *2. 5. Determination of the gadolinium concentration in nanogels by ICP-OES*

5 Gadolinium nanoparticle loading was determined on purified and concentrated
6 nanosuspensions by Inductively Coupled Plasma - Optical Emission Spectroscopy (ICP-
7 OES). The non-encapsulated complexes were separated from the NGs by high speed
8 centrifugation for 1 h 15 min at 4°C and 23 200 g (Beckman Avanti™ J-E Centrifuge,
9 France). The NP pellet was then incubated overnight in a 1:3 (v/v) mixture of HCl (37%) and
10 HNO₃ (69%) in order to release Gd from the polymer matrix and the complexes. After the NG
11 destruction, volumetric dilutions were carried out to achieve an appropriate Gd concentration
12 within the detection range of the method. Similar procedure was implemented to determine
13 Gd content in supernatants. Samples were analyzed using ICAP 6000 series ICP-OES
14 spectrometer. Counts of Gd were correlated to a Gd calibration curve generated by mixing
15 Gd(NO₃)₃ standard with unloaded NGs incubated under the same acidic conditions.

16 *2.6. Evaluation of fluorophore concentration in nanogels by fluorescence spectroscopy.*

17 Rhodamine or fluorescein concentrations were determined by fluorescence (Varian Cary
18 Eclipse spectrometer) on dialysed nanogels, after high speed centrifugation (23 200 g, 1 h 15,
19 4°C) both in NP pellets and in supernatants, using the same methodology as the one used for
20 the determination of fluorophore concentrations on CS-Rhod and CS-Fluo polymers.

21 *2.7. Relaxivity measurements*

22 *NMRD profiles.* ¹H NMRD profiles were measured on a Stellar Spinmaster FFC fast field
23 cycling NMR relaxometer (Stellar, Mede, Pavia, Italy) over a range of magnetic fields
24 extending from 0.24 mT to 0.7 T and corresponding to ¹H Larmor frequencies from 0.01 to 30
25 MHz using 0.6 mL samples in 10 mm o.d. tubes. The temperature was kept constant at 37°C.
26 An additional relaxation rate at 60 MHz was obtained with a Bruker Minispec mq60
27 spectrometer (Bruker, Karlsruhe, Germany). The diamagnetic contribution of unloaded
28 particles was measured and subtracted from the observed relaxation rates of the Gd-loaded
29 nanoparticles.

30 *MR Imaging.* MR imaging of NP suspensions were performed using a 3.0 T MRI device
31 (Skyra, Siemens Healthcare, Erlangen, Germany) with a 15 channel transmit/receive knee
32 coil. *T*₁-weighted images were obtained with an 3D fast spin-echo *T*₁ sequence (TR = 700 ms,
33 TE = 12 ms, FOV = 201×201 mm, matrix= 256×256, voxel size = 0.78×0.78×2mm). *T*₂-

1 weighted images were obtained with an 3D fast spin-echo T_2 sequence (TR = 1000 ms, TE =
2 103 ms, FOV = 199×199 mm, matrix = 384×384 , voxel size = $0.52 \times 0.52 \times 0.55$ mm). The
3 gadolinium concentrations were tested in the 25–200 μ M range.

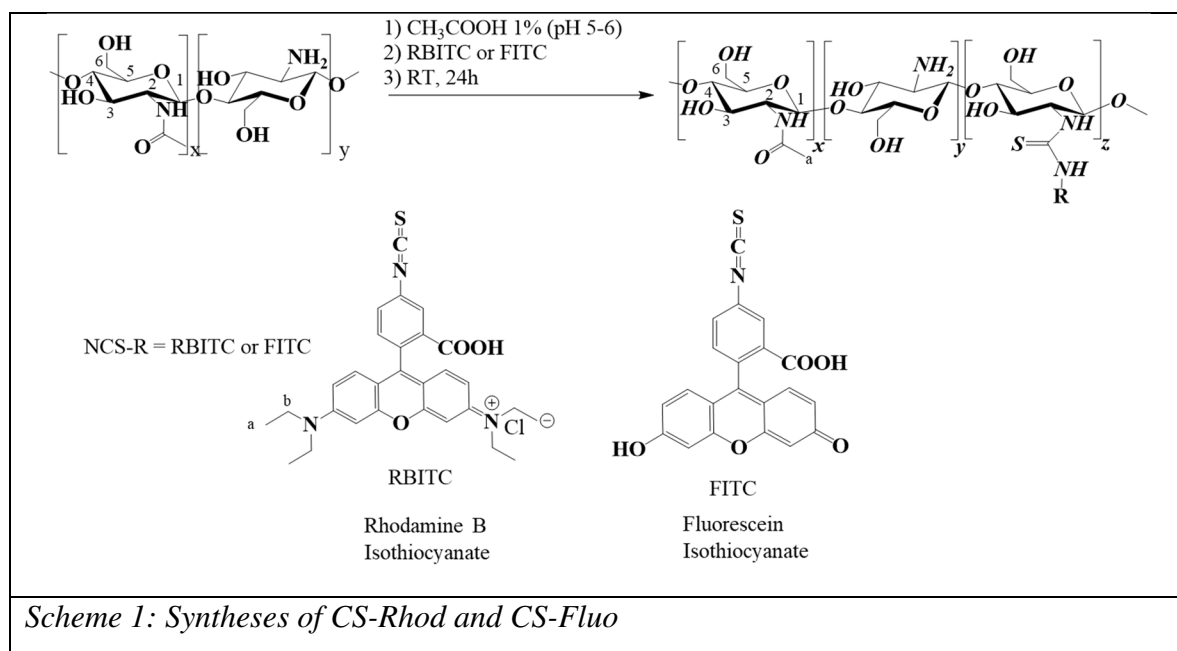
4

5

6

1 Results and Discussion

2 1.2. Preparation and characterization of CS grafted with Rhodamine B Isothiocyanate 3 (CS-Rhod) and Fluorescein Isothiocyanate (CS-Fluo)



4 The functionalization of chitosan (CS) by conventional fluorophores, namely RBITC and
5 FITC that emitted in red and green regions respectively, was performed by a direct coupling
6 between the fluorophore isothiocyanate group and the amino function of the CS glucosamine
7 residue. (Ma et al., 2018) To optimize the labelling procedure, several initial molar ratios
8 (NCS/ NH_2), chosen between 2 and 10% for each fluorophore, were used in order to provide
9 sufficient grafting yields while avoiding optical signal saturation. After workup and freeze-
10 drying, fluorescent CS samples were characterized by UV-visible and emission
11 spectroscopies, FT-IR and ^1H NMR at 318 K ($\text{D}_2\text{O}/\text{DCl}$ as solvent). The absorption and
12 fluorescence maxima in water medium of CS-Rhod were located at 550 nm and 576 nm,
13 respectively, and the ones of CS-Fluo were located at 450 nm and 511 nm, respectively
14 (Figure 1). They were similar to those of the free dyes (Leng et al., 2017; Xia et al., 2016).
15 FT-IR spectra of CS-Rhod and CS-Fluo samples (Figure S1) showed the disappearance of the
16 FT-IR band at $2030\text{-}2150\text{ cm}^{-1}$ attributed to the isothiocyanate group (Sinagaglia et al., 2012).
17 These data suggested the involvement of the thiourea moiety in the conjugation of both
18 fluorophores with CS.

19

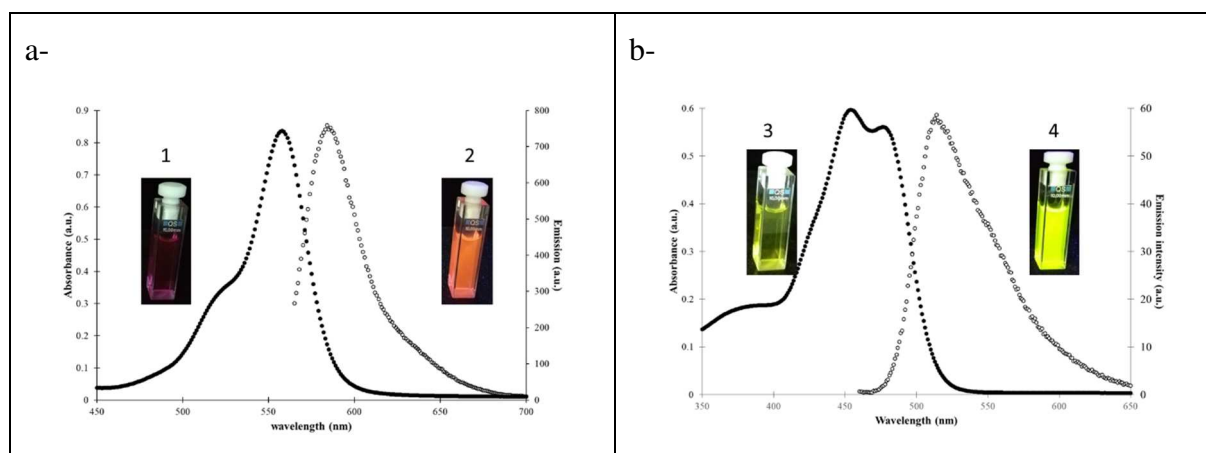


Figure 1: Absorbance (●) and emission (○) spectra of in acetate buffer (pH 4.7), (a) CS-Rhod; (b) CS-Fluo, % mol $(\text{NCS}/\text{NH}_2)_{\text{initial}} = 10\%$. Optical images of CS-Rhod and CS-Fluo under natural light (pictures 1 and 3, respectively) and under UV light (365 nm, pictures 2 and 4, respectively).

1 Similarly, ^1H NMR spectra of CS-Rhod and CS-Fluo (Figure S2), in addition to chemical
 2 shifts corresponding to CS backbone or acetyl protons (H_2 of pyranose ring at
 3 $\delta = 3.0$ ppm, H_3 to H_6 of pyranose ring at $\delta = 3.5\text{-}4.2$ ppm, anomeric H_1 at $\delta = 4.7$ ppm and
 4 acetyl protons at $\delta = 2.1$ ppm), confirmed the presence of rhodamine moiety in CS-Rhod
 5 samples (Figure S2a - H_a at $\delta = 1.3$ ppm, H_b at $\delta = 3.4$ ppm, and H_{ar} at $\delta = 6.9\text{-}7.9$ ppm) as
 6 well as fluorescein moiety in CS-Fluo samples (Figure S2b - H_{ar} at $\delta = 6.5\text{-}8.0$ ppm).
 7 In the absence of a spectroscopic marker specific to the thiourea linkage, the evaluation of CS
 8 degree of substitution (DS_{CS}) post-grafting, cannot be given by the sole ^1H NMR spectra
 9 analyses since they only help to determine the total amount of fluorophore associated to CS.
 10 Indeed, in CS-Rhod samples this amount (Rhod_T) could be determined by the ratio between
 11 the integration of H_a rhodamine ^1H signal (divided by 12) and chitosan signals (H_2 CS ^1H
 12 signal which was set to 1). Similar analysis could be performed for CS-Fluo, the total amount
 13 of fluorescein associated to CS (Fluo_T) being obtained *via* the ratio between the integration of
 14 fluorescein aromatic ^1H (divided by 9) and chitosan signals (H_2 CS ^1H signal always set to 1).
 15 Unfortunately for the lowest initial (NCS/NH_2) molar ratio (2%), the ^1H signals associated to
 16 each fluorophore were too weak to be integrated with accuracy. To circumvent this drawback,
 17 the total amount of each optical probe was determined by fluorescence and this, for each
 18 (NCS/NH_2) initial ratio (*Eq. 1* Experimental Section). The results obtained from fluorescence
 19 spectroscopy showed that after workup, the total amount of rhodamine (Rhod_T) associated to
 20 CS were 0.18, 0.44 and 1.03% for (NCS/NH_2) initial ratios of 2, 5 and 10%, respectively
 21 (Table S3), the total amount of fluorescein (Fluo_T) associated to CS being 0.22, 0.54 and
 22 1.02% for the same (NCS/NH_2) initial ratios, respectively. These data indicated then that only

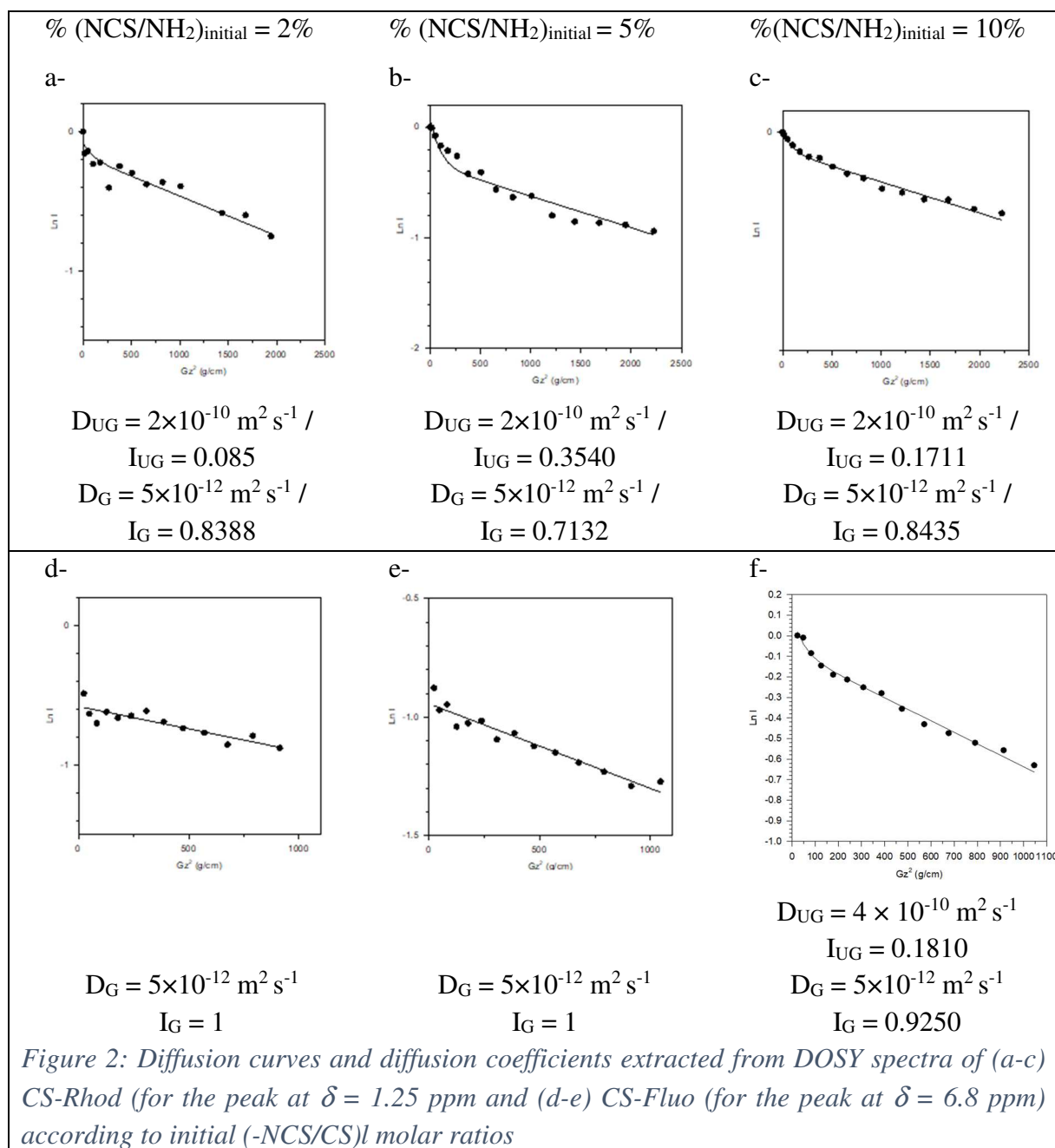
1 10% of the probe (Rhod or Fluo) initially introduced remained associated to CS after reaction,
2 which highlighted the efficiency of purification step.

3 In order to properly evaluate the amount of grafted fluorophore (Rhod_G or Fluo_G), CS-Rhod
4 and CS-Fluo samples were subjected to DOSY experiments (Belabassi et al., 2017).

5 In the case of CS-Rhod polymers, these curves extracted from CS-Rhod DOSY spectra were
6 clearly non-linear (Figures 2 a-c). Their biexponential shape highlighted in these samples the
7 presence of two contributions, one coming from the ungrafted rhodamine (Rhod_{UG}) which
8 diffused faster than the second one coming from grafted rhodamine to CS chains (Rhod_G).

9 Due to first the large difference between rhodamine and CS molecular weights and second
10 taking into account the weak percentages determined by fluorescence of fluorophores
11 associated to the polymer chains (*vide supra*), one can assume that fluorophore grafting
12 should not restrict CS chain mobility and consequently, CS-Rhod molecular weight must be
13 close to the one of CS. Therefore, a bi-exponential fitting of these curves was performed
14 (Eq.3), for which two diffusion coefficients of $2 \times 10^{-10} \text{ m}^2 \text{ s}^{-1}$ (for Rhod_{UG}, Figure S4) and
15 $5 \times 10^{-12} \text{ m}^2 \text{ s}^{-1}$ (for CS, Figure S4 and then CS-Rhod) were used.

16



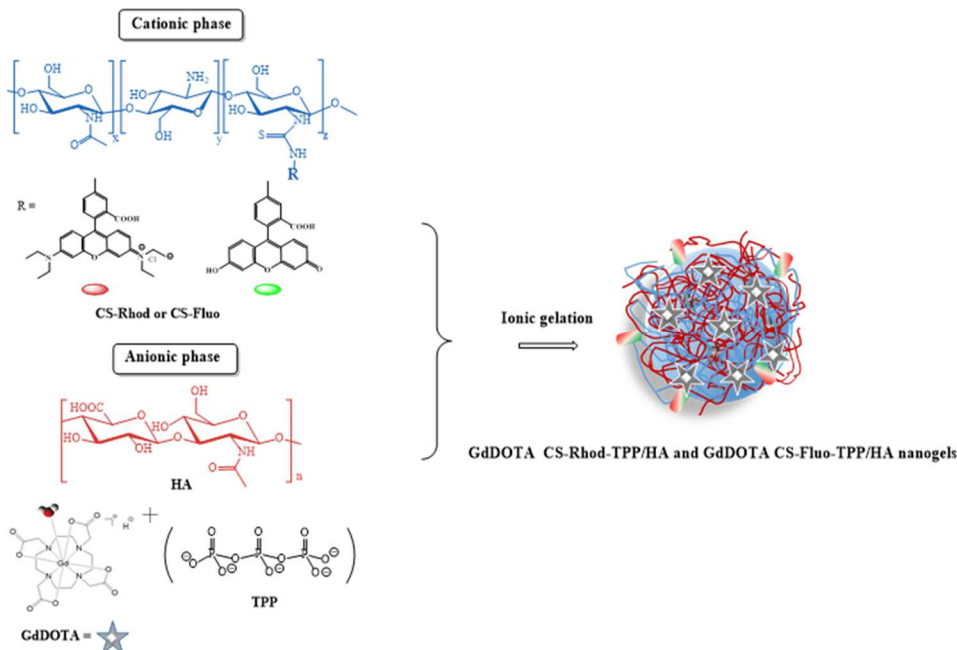
2 In the case of CS-Fluo polymers, the diffusion curves extracted from DOSY spectra were
3 linear for the two first ratios (2 and 5%) and clearly non-linear for the last one (10%) (Figures
4 2 d-f). For the two first cases, a mono-exponential fitting was considered (Eq.2) which led to a
5 diffusion coefficient close to the one measured on chitosan alone, meaning that 100 % of the
6 fluorophore present was grafted to chitosan. For the third one, a bi-exponential fitting was
7 performed for which two diffusion coefficients of $4 \times 10^{-10} \text{ m}^2 \text{ s}^{-1}$ (for Flu_{UG}, Figure S4) and
8 $5 \times 10^{-12} \text{ m}^2 \text{ s}^{-1}$ (for CS, Figure S4 and then CS-Fluo) were fixed. Thus, the curves fitting
9 allowed to extract the percentage of grafted fluorophore over their total amount
10 (Rhod_G/Rhod_T and Flu_G/Fluo_T, Eq. 4).

1 According to the initial molar ratio, Rhod_G/Rhod_T ratios were estimated between 67 and 91 %
 2 while Fluor_G / Fluor_T ratios were estimated between 84 and 100 % (Table S3). These results
 3 indicated that almost all the fluorophores present in fluorescent CS samples were grafted.
 4 Final DS_{CS}, as far as they are concerned, were comprised between 0.16 and 0.86 % (Table S3)
 5 whatever the fluorophore. This indicated that at least 1% of amino functions were
 6 functionalized with Rhod or Fluo, and that sufficient protonable amino functions remained
 7 available to be involved in the preparation of nanoparticles by ionic gelation.

8

9 *1.3. CS-Rhod-TPP/HA and CS-Fluo-TPP/HA nanogel syntheses and characterizations*

10 CS-Rhod with a DS_{CS} of 0.85% and CS-Fluo with a DS_{CS} of 0.86% were then evaluated for
 11 their ability to produce fluorescent CS-Rhod-TPP/HA and CS-Fluo-TPP/HA nanogels able to
 12 encapsulate gadolinium chelate. For that, CS-Rhod and CS-Fluo polymers in association with
 13 sodium hyaluronate (HA) in the presence of tripolyphosphate (TPP) were used to produce
 14 under mild conditions and without the use of solvents except water, nanoparticles by ionic
 15 gelation (Scheme 2). These conditions allowed the development of multivalent electrostatic
 16 interactions between the polycationic phase constituted of CS derivatives and the polyanionic
 17 chains of HA (ionic complexation between these polymers), these polymeric chains being
 18 interconnected by the low-molecular weight cross-linker, TPP. (Berger et al., 2004). With
 19 each polymer tested, stable and homogeneous nanosuspensions were obtained.



Scheme 2: CS-Rhod-TPP/HA and CS-Fluo-TPP/HA nanogel syntheses

1 Gadolinium-loaded nanoparticles were prepared in the same way by incorporating
 2 HGdDOTA as the MRI contrast agent in the preparation. This macrocyclic gadolinium
 3 chelate, characterized by a high thermodynamic and kinetic stability, is the active substance of
 4 DOTAREM®. It is recognized as low-risk towards nephrogenic systemic fibrosis (NSF) in
 5 renal impaired patients (Khawaja et al., 2015) and its macrocyclic structure helps to prevent
 6 gadolinium leakage and subsequent deposition in brain (Gianolio et al., 2017). The resulting
 7 GdDOTA_cCS-Rhod-TPP/HA or GdDOTA_cCS-Fluo-TPP/HA nanoparticles (Table 1) had
 8 similar morphological characteristics as the non-fluorescent ones (Table S5).

9 *Table 1: Intensity weighted (Z-average) diameters, polydispersity indexes (PdI), zeta potential*
 10 *(ζ) and Gd(III) loadings of CS-Rhod-TPP/HA and CS-Fluo-TPP/HA nanogels*

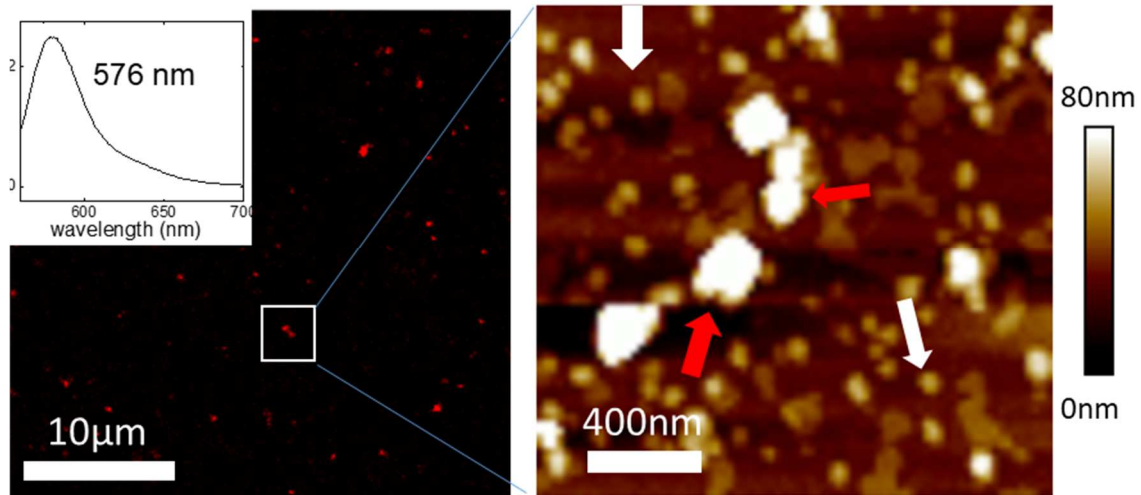
Polymer	Before dialysis			After dialysis				
	Z-ave \pm sd (nm)	PdI \pm sd	ζ \pm sd (mV)	Z-ave \pm sd (nm)	PdI \pm sd	ζ \pm sd (mV)	d_{AFM} \pm sd(nm)	[Gd] _{NP} (mM)
CS- Rhod	241 \pm 11	0.16 \pm 0.02	49 \pm 1	321 \pm 20	0.22 \pm 0.01	38 \pm 2	65 \pm 13	97
CS-Fluo	195 \pm 10	0.17 \pm 0.01	48 \pm 1	221 \pm 14	0.24 \pm 0.01	35 \pm 1	57 \pm 10	111
CS	219 \pm 10	0.20 \pm 0.01	43 \pm 4	226 \pm 10	0.19 \pm 0.01	35 \pm 1	62 \pm 12	96

11
 12 ICP-OES analyses of GdDOTA_cCS-Rhod-TPP/HA or GdDOTA_cCS-Fluo-TPP/HA
 13 nanoparticles indicated that their gadolinium loading, around 100 mM, was similar to those of
 14 GdDOTA_cCS-TPP/HA controls (Table 1).

15 To characterize the morphology and the optical properties of the fluorescent nanohydrogels,
 16 confocal images coupled to AFM measurements in liquid were used (Figure 3), thanks to a
 17 correlative setup. Compared to other types of microscopies, AFM allows to have a high
 18 resolution while keeping the proper physiological environment and then minimal physical
 19 perturbations to these fragile samples (which can burn under electronic irradiation for
 20 instance). From a methodological point of view, it was possible to check first the fluorescent
 21 properties of the NGs through confocal microscopy and then to focus on a proper area to get a

1 morphological characterization of the NGs by AFM. On Figure 3a, the confocal image and
2 the associated fluorescence spectrum with a maximum at 576 nm exhibited the expected
3 features for the HGdDOTA \subset CS-Rhod/HA/TPP NGs, confirming the fact that the NGs are
4 fluorescent. On Figure 3b, the same behavior was found for the HGdDOTA \subset CS-
5 Fluo/HA/TPP NGs with an emission at 511nm.

a-



b-

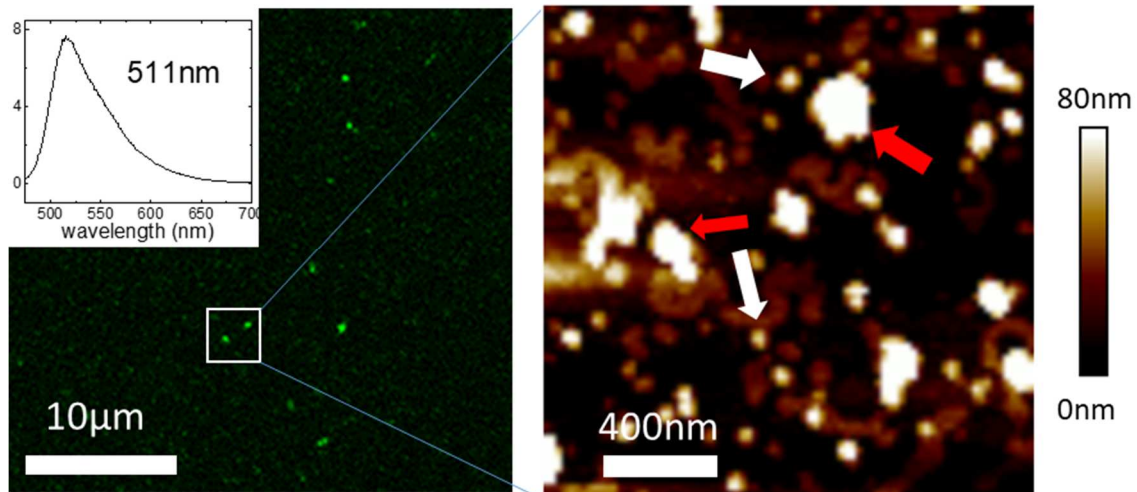


Figure 3: Confocal and associated AFM images of (a) HGdDOTA \subset CS-Rhod/HA/TPP NGs, and (b) HGdDOTA \subset CS-Fluo/HA/TPP NGs after dialysis.

6 Zooming with the AFM on a proper area allowed to show that, whatever the nanosuspensions,
7 the NGs were spherical particles and no significant morphological differences could be
8 noticed with a mix of isolated NPs (white arrows) or NG aggregates (red arrows). Whatever
9 the samples (with, or without HGdDOTA), the isolated NG diameters calculated from the
10 AFM images were inferior to 100 nm typically in the range of 60 nm (see Tables 1 and S5)

1 and the aggregates from 150 to 400 nm. Regarding the confocal images, the brighter and
2 larger spots could be attributed to the aggregates. As for the comparison with the DLS
3 measurements, such differences have already been observed for nanogels and could be
4 attributed to the fact that in DLS, because of the presence of aggregates, the response could be
5 biased by the use of mathematical models of signal processing (Rigaux et al., 2017).

6 Rhod and Fluo concentrations associated with nanogels were then determined by
7 fluorescence. Rhod and Fluo concentrations associated with GdDOTA₂-CS-Rhod-TPP/HA or
8 GdDOTA₂-CS-Fluo-TPP/HA NGs were 6.3 and 7.3 μ M respectively. Furthermore, emission
9 spectra of GdDOTA₂-CS-Rhod-TPP/HA or GdDOTA₂-CS-Fluo-TPP/HA nanosuspensions
10 were superimposable to those of unloaded CS-Rhod-TPP/HA or CS-Fluo-TPP/HA nanogels
11 (Figure S6), which showed that the presence of HGdDOTA within the nanoparticles did not
12 perturb their fluorescent response. As shown above (Figure 3), confocal microscopy images
13 of nanogels confirmed that all the CS-Rhod-TPP/HA or CS-Fluo-TPP/HA NGs were red and
14 green emitters respectively.

15 Before testing the effectiveness of GdDOTA₂-CS-Rhod-TPP/HA and GdDOTA₂-CS-Fluo-
16 TPP/HA NGs in enhancing the MRI signal, their potential cytotoxicity towards cells, was
17 evaluated by means of MTT and LDH assays (Figure 4) (Fotakis & Timbrel 2006). For that, a
18 murine macrophage cell line (RAW 264.7) was chosen, since macrophages are among the
19 major cells mediating the inflammatory response to foreign substances, especially
20 nanoparticles (Jiang et al. 2017). A20 cells which are lymphocyte cells were chosen as they
21 are involved in the immune system (Gheran et al. 2017).

22

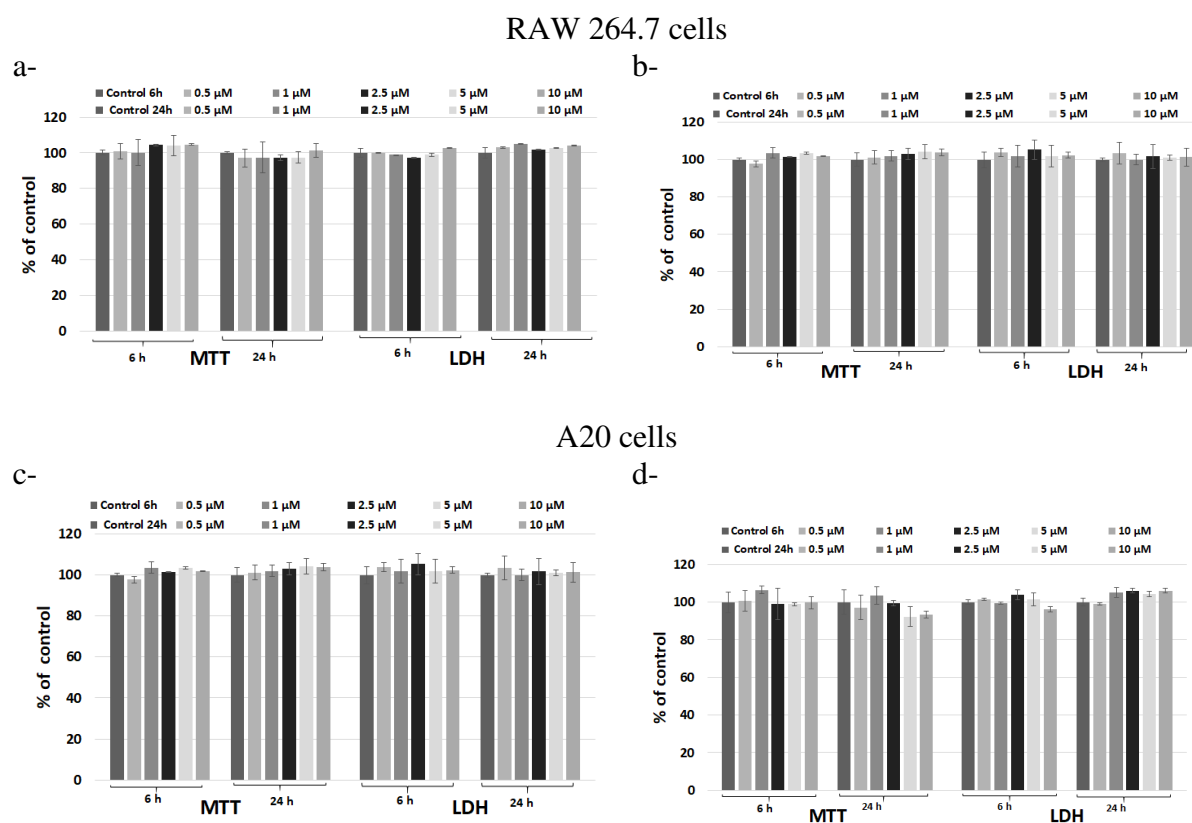


Figure 4: Cell viability and cytotoxicity established by MTT and LDH assays in the presence of RAW 264.7 cells and A20 cells after exposure to 0.5, 1, 2.5, 5 and 10 μM Gd of a and c - GdDOTA_c-CS-Rhod-TPP/HA and b and d- GdDOTA_c-CS-Fluo-TPP/HA NGs for 6 and 24 hours. Results are calculated as means \pm sd ($n = 3$) and expressed as % from controls (untreated cells).

- 1 The exposure of RAW264.7 and A20 cells to fluorescent Gd nanogels did not affect the cell
- 2 survival. Furthermore, this absence of toxicity is similar to the one observed for the non-
- 3 fluorescent analogues (Gheran et al. 2018, Gheran et al. 2017) which highlighted that
- 4 fluorophore grafting, while providing additional imaging functionality, did not affect the
- 5 harmlessness of nanogels to cells.

- 6 Finally, in order to evaluate the MRI efficiency of GdDOTA_c-CS-Rhod-TPP/HA and
- 7 GdDOTA_c-CS-Fluo-TPP/HA NGs, their longitudinal relaxation rates were recorded at 37°C,
- 8 as a function of resonance frequency. The corresponding NMR dispersion profiles (NMRD)
- 9 (Figure 5) revealed a maximum in relaxivity between 25 and 30 MHz
- 10 ($r_1 \geq 80 \text{ mM}^{-1}\text{s}^{-1}$) by comparison to GdDOTA relaxivity in the same field region
- 11 ($r_1 \sim 3.5 \text{ mM}^{-1}\text{s}^{-1}$ at 20 MHz) (Idée et al. 2006).

12

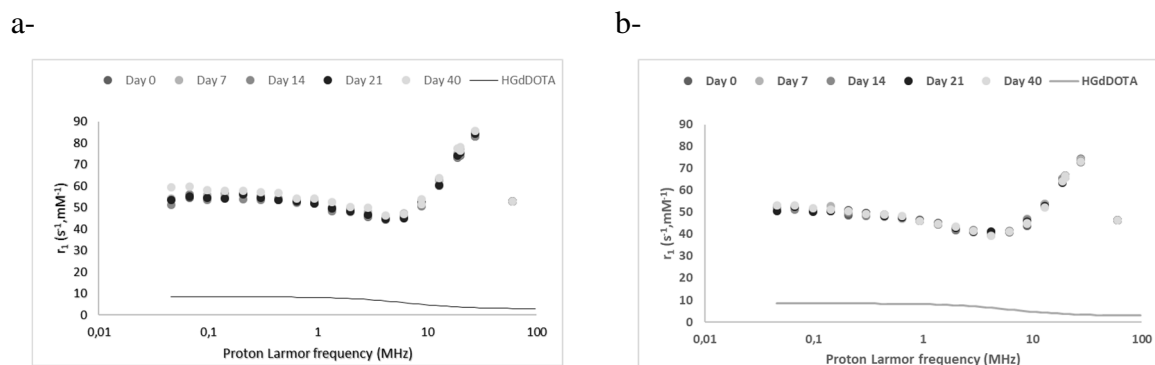


Figure 5: NMRD relaxivity profiles of a- GdDOTA_cCS-Rhod-TPP/HA NGs and b- GdDOTA_cCS-Fluo-TPP/HA NGs and their evolution over time (37°C)

1 These profiles shapes were typical of Gd chelate with a restricted rotational motion (Merbach,
 2 Helm & Toth, 2013). Indeed, the spatial confinement of GdCAs within nanohydrogels
 3 allowed to slow-down their tumbling motion. Furthermore, the hydrophilic nature of CS and
 4 HA (Basu et al., 2015) that constituted the nanogel polymer matrix allowed the optimization
 5 of water residence times in the gadolinium coordination sphere, leading to a strong outer-
 6 sphere and/or second-sphere contribution to the relaxivity. Moreover, one should notice that
 7 each profile shape was maintained over a period of 40 days (Figure 5), which demonstrated
 8 the stability of GdDOTA_cCS-Rhod-TPP/HA and GdDOTA_cCS-Fluo-TPP/HA nanogels as
 9 well as their ability to contain their Gd loading over the time.

10 In order to check how this relaxation amplification could be translated into magnified MR
 11 images, T_1 - and T_2 -weighted images of phantoms containing GdDOTA_cCS-Rhod-TPP/HA
 12 and GdDOTA_cCS-Fluo-TPP/HA suspensions were acquired on a 3T clinical imager, with
 13 DOTAREM® as control (Figure 6).

14

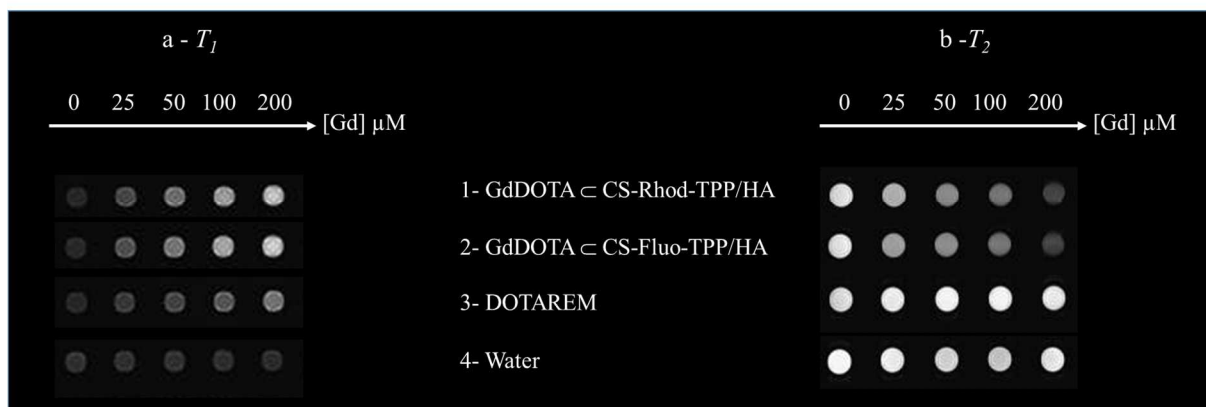


Figure 6: a) T_1 - and b) T_2 - weighted images of $GdDOTA \subset CS-Rhod-TPP/HA$ (line 1) and $GdDOTA \subset CS-Fluo-TPP/HA$ NPs (line 2), DOTAREM® (line 3) and water (line 4) as controls. All samples were imaged at 3T, 37°C with 3D fast spin echo T_1 or T_2 sequences.

1 For the T_1 -weighted images, the bright signal enhancement progressively increased with
 2 increased gadolinium concentrations in nanogels. Comparison with DOTAREM® control
 3 showed that the signal enhancement was due to the incorporation of GdDOTA within the
 4 fluorescent CS-TPP/HA nanogels. Indeed, encapsulation of large amounts of GdDOTA in
 5 nanogels resulted in an apparent increase in the mass of the complex and then in a restriction
 6 of its rotational motion, which was responsible for the exaltation of the relaxivity (Merbach et
 7 al. 2013). Conversely for the T_2 -weighted images, under the same conditions, image
 8 darkening was observed. This important T_2 effect at high magnetic field results from the slow
 9 rotation of the encapsulated complexes and/or magnetic susceptibility effects (Aime et al.,
 10 2007). As a result, these images corroborated relaxometric measurements and confirmed the
 11 dual T_1/T_2 properties of the gadolinium loaded nanogels.

12

13 2. Conclusion

14 In this paper, we reported the synthesis and the characterization of a series of fluorescent
 15 chitosans and the subsequent synthesis of biocompatible nanohydrogels by ionic gelation in
 16 the presence of hyaluronic acid. MRI and optical imaging modalities were set within the
 17 nanogels thanks to chitosan and encapsulation of Gd chelate during the process. The low
 18 degree of substitution of chitosans by fluorophores and the hypersensitive MRI character of
 19 Gd chelate buried within the nanoparticles allowed to take into account the differences in
 20 sensibility between MRI and optical imaging modalities, so as to obtain an optimal signal in
 21 both modalities. Both MRI and optical imaging activities were evaluated. T_1 and T_2 -weighted

1 phantom MR images of nanogels, recorded on a 3T clinical scanner, showed an increase in
2 image contrast for lesser Gd doses, by comparison to those used with DOTAREM®. The huge
3 content of water and the presence of Gd chelate within the nanogels did not seem to quench
4 their emission. This absence of quenching was demonstrated in fluorescence imaging by their
5 red or green emission. Further work is in progress in order to produce CS-TPP/HA
6 nanohydrogels able to combine multicolor optical coding for multiplexing and magnetic
7 properties.

8

9 **ACKNOWLEDGEMENTS**

10 Yarong Shi (Bruker Nano, Inc, Santa Barbara, CA 93117, USA and LRN EA4682,
11 University of Reims Champagne Ardenne), Christine Terryn (PICT platform, University of
12 Reims Champagne-Ardenne) and Christophe Portefaix (Radiology Department, CHU de
13 Reims – Hôpital Maison Blanche) are gratefully acknowledged for their help in AFM
14 measurements, optical imaging and MRI experiments respectively.

15 The authors would like to thank the “Programme de coopération transfrontalière Interreg
16 France-Wallonie-Vlaanderen” for funding the “Nanocardio” project (<http://nanocardio.eu>) and
17 the post-doctoral fellowship of V. Malyskyi, the PHC Brancusi program (project n°
18 43465WA) and the PIAnET platform (supported by the European Regional Development
19 Fund and the Region Champagne Ardenne). This work was also performed with the financial
20 support of the FNRS, FEDER, the ARC, the Walloon Region (Biowin and Interreg projects)
21 and the COST actions. Authors thank the Center for Microscopy and Molecular Imaging
22 (CMMI, supported by European Regional Development Fund Wallonia) and the Bioprofiling
23 platform (supported by the European Regional Development Fund and the Walloon Region,
24 Belgium). Finally, this work was supported by a grant of the Romanian Ministry of Research
25 and Innovation, CCCDI-UEFISCDI, project number PN III-P3-3.1-PM-RO-FR-2019-
26 0204/6BM/2019, within PNCDI III.

27

28 **REFERENCES**

29 Aime, S., Delli Castelli, D., Lawson, D.& Terreno, E. (2007) Gd-loaded liposomes as T1,
30 susceptibility, and CEST agents, All in One. *J. Am. Chem. Soc.*, 129 (9), 2430-2431.
31 Asberg, P., Nilsson, P.& Inganas, O. Fluorescence quenching and excitation transfer between
32 semiconducting and metallic organic layers. *J. Appl. Phys.*, 96 (6), 3140.

1 Augé, S., Amblard-Blondel, B. & Delsuc, M. A. (1999). Investigation of the diffusion
2 measurement using PFG and tTest r against experimental conditions and parameters. *J. Chim.*
3 *Phys. Phys.-Chim. Biol.*, 96(9–10), 1559–1565.

4 Basu, A., Kunduru, K. R., Abtew, E. R. & Domb, R. T. (2015). Polysaccharide-Based
5 Conjugates for Biomedical Applications. *Bioconjugate Chem*, 26(8), 1396 – 1412.

6 Belabassi, Y., Moreau, J., Gheran, V., Henoumont, C., Robert, A., Callewaert, M., Rigaux,
7 G., Cadiou, C., Vander Elst, L., Laurent, S., Muller, R. N., Dinischiotu, A., Voicu, S. N. &
8 Chuburu, F. (2017). Synthesis and characterization of PEGylated and fluorinated chitosans:
9 application to the synthesis of targeted nanoparticles for drug delivery. *Biomacromolecules*,
10 18(9), 2756–2766.

11 Berger, J., Reist, M., Mayer, J. M., Felt, O., Peppas, N. A. & Gurny, R. (2004). Structure and
12 interactions in covalently and ionically crosslinked chitosan hydrogels for biomedical
13 applications. *Eur. J. Pharm. Biopharm.*, 57, 19-34.

14 Callewaert, M., Roullin, V. G., Cadiou, C., Millart, E., Van Gulik, L., Andry, M. C.,
15 Portefaix, C., Hoeffel, C., Laurent, S., Vander Elst, L., Muller, R., Molinari, M., & Chuburu,
16 F. (2014). Tuning the composition of biocompatible Gd nanohydrogels to achieve
17 hypersensitive dual T1/T2 MRI contrast agents. *J. Mater. Chem. B*, 2 (37), 6397–6405.

18 Courant, T., Roullin, V. G., Cadiou, C., Callewaert, M., Andry, M. C., Portefaix, C., Hoeffel,
19 C., de Goltstein, M. C., Port, M., Laurent, S., Vander Elst, L., Muller, R., Molinari, M., &
20 Chuburu, F. (2012). Hydrogels Incorporating GdDOTA: Towards Highly Efficient Dual
21 T1/T2 MRI Contrast Agents. *Angew. Chem., Int. Ed. Engl.*, 51(36), 9119–9122.

22 Fotakis, G. & Timbrell, J. A. (2006). In vitro cytotoxicity assays: Comparison of LDH,
23 neutral red, MTT and protein assay in hepatoma cell lines following exposure to cadmium
24 chloride. *Toxicol. Lett.*, 160, 171–177.

25 Gheran, C.V., Voicu, S.N., Rigaux, G., Callewaert, M., Chuburu, F., & Dinischiotu, A.
26 (2017). Biological effects induced by Gadolinium nanoparticles on Lymphocyte A20 cell line.
27 *The EuroBiotech Journal*, 1, 57–64.

28 Gheran, C. V., Rigaux, G., Callewaert, M., Berquand, A., Molinari, M., Chuburu, F., Voicu,
29 S. N., & Dinischiotu, A. (2018). Biocompatibility of Gd-Loaded Chitosan-Hyaluronic Acid
30 Nanogels as Contrast Agents for Magnetic Resonance Cancer Imaging. *Nanomaterials*, 8(4),
31 201.

32 Gianolio, E., Bardini, P. Arena, F., Stefania, R. Di Gregorio, E., Iani, R. & Aime, S. (2017).
33 Gadolinium retention in the rat brain: assessment of the amounts of insoluble gadolinium-

1 containing species and intact gadolinium complexes after repeated administration of
2 gadolinium-based contrast agents. *Radiology*, 285(3), 839–849.

3 Gupta, A., Caravan, P., Price, W. S., Platas-Iglesias, C., & Gale, E. M. (2020). Applications
4 for transition-metal chemistry in contrast-enhanced magnetic resonance imaging. *Inorg.*
5 *Chem.*, 59, 6648-6678.

6 Gupta, K. C. & Jabrail, F.H. (2006). Preparation and characterization of sodium hexameta
7 phosphate cross-linked chitosan microspheres for controlled and sustained delivery of
8 centchroman. *Int. J. Biol. Macromol.*, 38, 272-283.

9 Hirai, A., Odani, H., & Nakajima, A (1991). Determination of Degree of Deacetylation of
10 Chitosan by H NMR Spectroscopy. *Polymer. Bulletin*, 26(1), 87–94.

11 Idée, J. M., Port, M., Raynal, I., Schaefer, M., Le Greneur, S. & Corot, C. (2006).
12 *Fundamental & Clinical Pharmacology*, 20, 563-576.

13 Johnson, C. S, Jr. (1999). Diffusion Ordered Nuclear Magnetic Resonance Spectroscopy:
14 Principles and Applications. *Prog. Nucl. Magn. Reson. Spectrosc*, 34(3–4), 203–256.

15 Jiang, L.Q., Wang, T.Y., Webster, T.J., Duan, H.J., Qiu, J.Y., Zhao, Z.M., & Zheng, C.L.
16 (2017). Intracellular disposition of chitosan nanoparticles in macrophages: intracellular
17 uptake, exocytosis, and intercellular transport. *Int. J. Nanomed.*, 12, 6383-6388.

18 Kanda, T., Oba, H., Toyoda, K., Kitajima, K., & Furui, S. (2016). Brain gadolinium
19 deposition after administration of gadolinium-based contrast agents. *Jpn. J. Radiol.*, 34, 3-9.

20 Khawaja, A. Z., Cassidy, D. B., Al Shakarchi, J., McGrogan, D. G., Inston, N. G., & Jones, R.
21 G. (2015). Revisiting the risks of MRI with Gadolinium based contrast agents—review of
22 literature and guidelines. *Insights Imaging*, 6, 553–558.

23 Leng, T., Jakubek, Z. J., Mazloumi, M., Leung, A. C. W., & Johnston, L. J. (2017). Ensemble
24 and Single Particle Fluorescence Characterization of Dye-Labeled Cellulose Nanocrystals.
25 *Langmuir*, 33(32), 8002–8011.

26 Lux, J., Chan, M., Van der Elst, L., Schopf, E., Mahmoudi, S., Laurent, S., & Almutairi A.
27 (2013). Metal chelating crosslinkers form nanogels with high chelation stability. *J. Mater.*
28 *Chem. B*, 1, 6359-6354.

29 Ma, O., Lavertu, M., Sun, J., Nguyen, S., Buschmann, M. D., Winni, F. M., & Hoemann, C.
30 D. (2008). Precise derivatization of structurally distinct chitosans with rhodamine B
31 isothiocyanate. *Carbohydr. Polym.*, 72(4), 616–624.

32 Mei, S., Zhou, J., Sun, H-T., Cai, Y., Sun, L-D., Jun, D.& Yan, C-H. (2021). Networking state
33 of ytterbium ions probing the origin of luminescence quenching and activation in
34 nanocrystals. *Adv. Sci.*, 8(6), 2003325.

1 Merbach, A. E., Helm, L., & Toth, E. (2013). *The Chemistry of Contrast Agents in Medical*
2 *Magnetic Resonance Imaging* (2nd Ed.) Chichester: Wiley and Sons).

3 Rigaux, G., Gheran, C. V., Callewaert, M., Cadiou, C., Voicu, S. N., Dinischiotu, A., Andry,
4 M. C., Vander Elst, L., Laurent, S., Muller, R. N., Berquand, A., Molinari, M., Huclier-
5 Markai, S., & Chuburu, F. (2017). A multi-technique approach combining DLS, AF4 and
6 AFM in liquid mode to select Gd-loaded chitosan-TPP nanohydrogels for MRI positive
7 contrast agent for Lymph Node Imaging. *Nanotechnology*, 28, Article ID 055705.

8 Rogosnitzky, M. & Branch, S. (2016). Gadolinium-based contrast agent toxicity: a review
9 of known and proposed mechanisms. *Biometals*, 29 (3) 365–376.

10 Sang, Z., Quan, J., Han, J., Deng, X., Shen, J., Li, G. & Xie, Y. (2020). Comparison of three
11 water-soluble polyphosphate tripolyphosphate, phytic acid, and sodium hexametaphosphate as
12 crosslinking agents in chitosan nanoparticle formulation. *Carbohydrate Polymers*, 230,
13 115577.

14 Sinagaglia, G., Magro, M., Miotto, G., Cardillo, S., Agostinelli, E., Zboril, R., Bidollari, E., &
15 Vianello, F. (2012). Catalytically active bovine serum amine oxidase bound to fluorescent and
16 magnetically drivable nanoparticles. *Int. J. Nanomed.*, 7, 2249–2259.

17 Soleimani, A., Martinez, F., Economopoulos, V., Foster, P. J., Scholl, T. J., & Gillies, E. R.
18 (2013). Polymer cross-linking: a nanogel approach to enhancing the relaxivity of MRI
19 contrast agents. *J. Mater. Chem. B.*, 1, 1027-1034.

20 Vårum, K. M., Antohonsen, M. W., Grasdalen, H., & Smidsrød, O (1991). Determination of
21 the Degree of N-Acetylation and the Distribution of N-Acetyl Groups in Partially N-
22 Deacetylated Chitins (Chitosans) by High-Field NMR Spectroscopy. *Carbohydr. Res.*, 211,
23 17–23.

24 Washner, J., Gael, E. M., Rodriguez-Rodriguez, A., & Caravan, P. (2019). Chemistry of MRI
25 contrast agents: current challenges and new frontiers. *Chem. Rev.*, 119, 957-1057.

26 Xia, S., Yang, H., Duan, L., Gao, G. H., & Zhang, X. (2016). A potential dual-modality optical
27 imaging probe based on the pH-responsive micelle. *J. Polym. Res.*, 23, 179.

28

Graphical abstract

